Thermal Stress Cracking of Sliding Gate Plates

Hyoung-Jun Lee[1], Seong-Mook Cho[1], Seon-Hyo Kim[1], Brian G. Thomas[2]
Sang-Woo Han[3], Tae-In Chung[3], Joo Choi[3]

[1]Department of Materials Science and Engineering,
Pohang University of Science and Technology,
San 31, Hyoja-Dong, Nam-Gu, Pohang, Gyeongbuk, 790-784, South Korea
Phone: +82-54-279-5968
Fax: +82-54-279-2399
E-mail: leehjun@postech.ac.kr, y104401@postech.ac.kr, seonhyo@postech.ac.kr

[2]Department of Mechanical Science and Engineering,
University of Illinois at Urbana-Champaign,
1206 W. Green St., Urbana, IL, 61801, USA
Phone: +1-217-333-6919
Fax: +1-217-244-6534
E-mail: bgthomas@uiuc.edu

[3]Steel Making Research Group,
POSCO Technical Research Laboratories, POSCO
Dongchon-Dong, Nam-Gu, Pohang, Gyeongbuk, 790-785, South Korea
Phone: +82-54-220-2890
Fax: +82-54-220-6832
E-mail: nedahsw@posco.com, tichung0428@posco.com, choijoo@posco.com

Key words: Refractory, Friction force, Pre-heating, Finite-element, Computational model

ABSTRACT

The sliding gate plate that controls steel flow through the tundish nozzle sometimes cracks leading to air aspiration and safety concerns. To evaluate possible mechanisms for crack formation, this research applies a 3-D finite-element model of the thermal and mechanical stress in a sliding-gate plate during preheating and casting induced by thermal expansion and/or mechanical movement. The thermal model is first validated with previous temperature histories measured during preheating and casting in a ladle plate. The model of a tundish sliding gate nozzle is then used to investigate thermal-mechanical behavior and cracking due to the temperature variations during preheating and casting. The model predictions of the maximum stress location and orientation match well with the crack location observed in used plates from POSCO. Different mechanisms for the formation of two different types of common through-thickness cracks are identified and explained. The first involves exterior tensile stress during heating stages, and the second is due to excessive compression from non-optimal placement of guide points on the steel cassette.

INTRODUCTION

Flow between the tundish and mold in continuous-steel casting is often controlled by an assembly of three refractory plates, as shown in Figure 1. The middle plate is moved to adjust the opening to control the flow rate through the nozzle to maintain a stable mold meniscus level. Cracking of the sliding gate refractories is important because it poses a great potential safety hazard, in addition to steel quality problems. Even if cracks are rare, the precautionary limits put on lifetimes and productivity to avoid potential problems

may be very costly. Furthermore, through-thickness cracks may lead to inclusion problems in the steel, due to re-oxidation from air aspiration through the cracks. Radial through-thickness cracks are common, such as shown in the slide gate plates in Figure 2-a) and b). The white, inverted triangular-shaped area circled in red on the fracture surface of the through-thickness crack surface in Figure 2-d) indicates that graphite in the sliding gate plate has been oxidized, suggesting that the steel was likely oxidized as well. Figure 2-c) shows some less-common transverse cracks.

Previous research has investigated refractory composition effects to extend service life and achieve higher productivity [1, 2]. Due to their inherent brittleness, refractories are subject to cracking problems, but the detailed mechanisms and relative importance of the different stress sources have received little attention. When refractories are subjected to high heat transfer and rapid changes in temperature during pre-heating and casting, the resulting thermal stress may cause cracks [3]. Another source of stress is the mechanical load provided to the plates and cassette by the bolts, which may be non-uniform and create high localized surface pressure [1]. Also, friction forces are generated by the horizontal (back and forth) movements of the middle sliding plate. Finally, ferrostatic pressure due to height difference between tundish free surface and sliding gate location provides additional load.

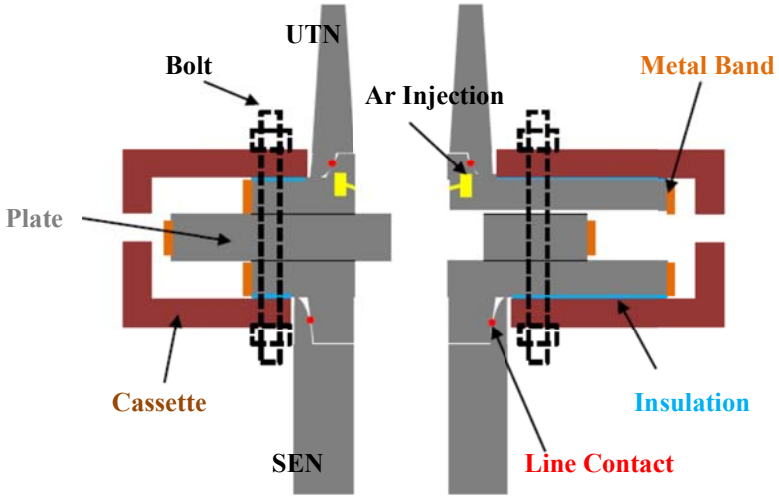

Figure 1. Schematic of sliding gate nozzle system

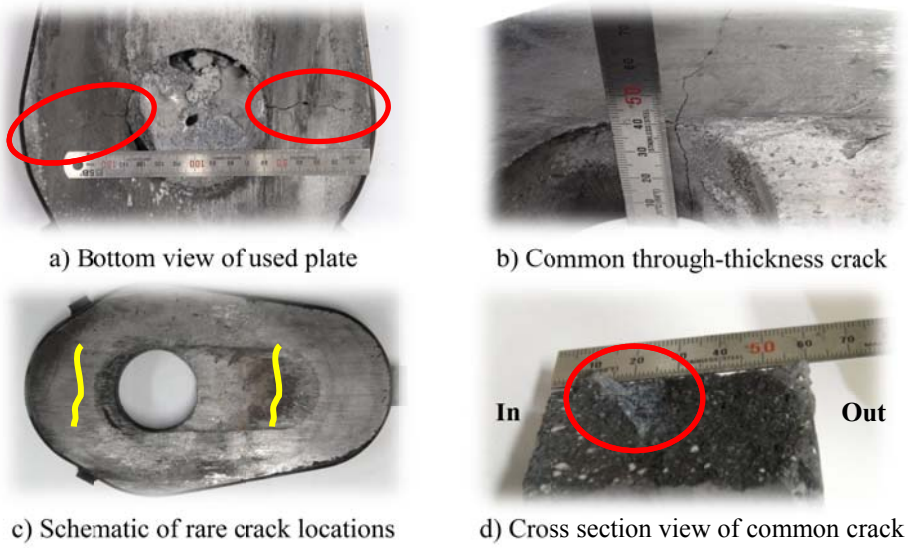

a) Bottom view of used plate
b) Common through-thickness crack
c) Schematic of rare crack locations
d) Cross section view of common crack

Figure 2. Different cracks in sliding gate plates

COMPUTATIONAL MODEL

To explore thermal and mechanical stress in a sliding gate plate during preheating and casting, a three-dimensional thermal-stress model was developed. Temperature, $T(x)$, of the components of the sliding gate assembly is found by solving the heat-conduction equation [4].:

$$k\nabla^2 T = 0 \tag{1}$$

where k is the thermal conductivity, and x are the three coordinate directions. The mechanical behavior is found by solving the differential equations of force equilibrium:

$$\nabla \cdot \boldsymbol{\sigma} = F \tag{2}$$

where F if the force vector from thermal, mechanical, and ferrostatic pressure loads, $\boldsymbol{\sigma}(x)$ is the Cauchy stress tensor, computed by Hooke's law of elasticity:

$$\boldsymbol{\sigma} = \boldsymbol{C} : \boldsymbol{\varepsilon}^{el} \tag{3}$$

where $\boldsymbol{C}$ is the fourth-order tensor containing 81 elastic coefficient.:

$$C_{ijkl} = \frac{E}{2(1+\nu)}\left(\delta_{ik} + \delta_{jl}\right) + \frac{\nu E}{(1+\nu)(1-2\nu)}\delta_{ij}\delta_{kl} \tag{4}$$

where E is Young's modulus, 65 GPa for refractory and 206 GPa for the steel cassette; ν is Poisson's ratio, 0.2 for refractory and 0.3 for the steel cassette; and δ_{ij} is the Kronecker delta. The elastic strain tensor $\boldsymbol{\varepsilon}^{el}(x)$ is computed from an additive decomposition of the strains:

$$\boldsymbol{\varepsilon}^{el} = \boldsymbol{\varepsilon} - \boldsymbol{\varepsilon}^{th} \tag{5}$$

where $\boldsymbol{\varepsilon}(x)$ is the total strain tensor, computed from the gradient of the displacement field $\boldsymbol{u}(x)$:

$$\varepsilon = \frac{1}{2}\left(\nabla \boldsymbol{u} + (\nabla \boldsymbol{u})^T\right) \tag{6}$$

and $\boldsymbol{\varepsilon}^{th}(x)$ is the thermal strain tensor, calculated based on the coefficient of thermal expansion α and reference temperature T_0:

$$\varepsilon^{th} = \alpha(T - T_0)\boldsymbol{I} \tag{7}$$

where $\boldsymbol{I} = \delta_{ij}$ is the second-order identity tensor, and α is thermal expansion coefficient, 8.2×10^{-6} °C^{-1} for refractory.

For the thermal problem, the flame and molten steel heat convection boundary conditions in the ladle and tundish sliding gate nozzle:

$$-k\nabla T \cdot \boldsymbol{n} = h(T - T_\infty) \tag{8}$$

where $\boldsymbol{n}(x)$ is the surface normal to outside, $h(x)$ is the convection heat transfer coefficient and $T_\infty(x)$ is the sink temperature. During the preheating stage, internal gas flame temperature and heat transfer coefficient are needed. Based on liquefied natural gas (LNG), containing 88% Methane (CH_4), 5% Ethane (C_2H_6), 5% Propane (C_3H_8) and 2 % Butane (C_4H_6) [5], and stoichiometric air, a flame temperature model [6] gives a gas temperature of 1518 °C with no excess air. However, the flames do not directly touch the sliding gate plates and there are heat losses due to excess air entrainment, so the internal gas temperature was assumed to be 750 °C.

During preheating, the heat transfer coefficient for free heat convection from the exterior of the cylinder-shaped nozzle to atmosphere is given by the relation for turbulent flow by Churchill et al. [7]:

$$\overline{Nu}_D = \left\{ 0.825 + \frac{0.387 Ra^{1/6}}{[1 + (0.492/\mathrm{Pr})^{8/27}]} \right\}^2 \qquad h = \frac{Nu \cdot k}{2r} \tag{9}$$

where Nu is Nusselt number, Ra is Rayleigh number, Pr is Prandtl number, h is free heat transfer coefficient, k is thermal conductivity and r is nozzle outside radius, of 0.225 m. This gives a free heat transfer coefficient ($h_{o,preheat}$) of 8.8 W/m^2·K.
During preheating, the heat transfer coefficient for forced heat convection from the turbulent flowing combustion products to the contact surfaces on the nozzle interior are given by an empirical equation for smooth cylinders by Petukhov et al.[8]:

$$Nu = \frac{[(f/8)\,\mathrm{Re}_D\,\mathrm{Pr}]}{[1.07 + 12.7(f/8)^{1/2}(\mathrm{Pr}^{2/3} - 1)]} \qquad h = \frac{Nu \cdot k}{2r} \tag{10}$$

where Re_D is the Reynolds number and f is Darcy friction factor. This gives $h_{i,preheat}$ of 65 W/m^2·K

During the steel casting stage, the combustion gases are replaced by molten steel, flowing through the sliding gate bore at 1550°C. The forced convection relation for turbulent metal flow from Sleicher and Rouse equation[9] is used:

$$\mathrm{Re} = \frac{2ur}{\upsilon} \quad \mathrm{Pr} = \frac{\upsilon}{\alpha} \quad a = 0.88 - \frac{0.24}{4 + \mathrm{Pr}} \quad b = \frac{1}{3} + 0.5\exp(-0.6\,\mathrm{Pr}) \quad Nu = 5 + 0.015\,\mathrm{Re}^a\,\mathrm{Pr}^b \quad h = \frac{Nu \cdot k}{2r} \tag{11}$$

where u is an average flow velocity in cross sectional area of cylinder, ν is kinematic viscosity of molten steel and a and b vary with Nusselt number. This gives $h_{i,steel}$ of 28.7 kW/m^2·K.

The heat conduction boundary conditions of the sliding plates are:

$$-k\nabla T \cdot \boldsymbol{n} = q \cdot \boldsymbol{n} \tag{12}$$

where $q(x)$ is the heat flux vector. The boundary conditions of the radiation heat loss from the heated sliding gate plates:

$$-k\nabla T = \varepsilon\sigma\left(T^4 - T_{sur}^4\right) \tag{13}$$

where ε is the emissivity of materials and σ is the Stefan-Boltzmann constant.

Mechanical loading is applied by constraining the horizontal displacements of the refractory plates where they touch the guide points on the steel cassette. Additional mechanical loading pressure in the vertical direction is provided by tension in the bolts where they contact the plates, but this was ignored in the current work.

Ferrostatic pressure is imposed on the inside refractory surfaces exposed to the flowing steel:

$$F_p = \rho g h \tag{14}$$

where h is height difference between the tundish free surface and the sliding gate location, 1.8 m, ρ is molten steel density, 7020 kg/m^3, g is gravitational acceleration 9.81 m/s^2 and F_p is the resulting average ferrostatic pressure, 0.124 MPa. Relative to the typical stress from thermal expansion, $-E \cdot \alpha \cdot \Delta T$, which for 1000 °C temperature change is ~540 MPa, this ferrostatic pressure is negligible and so can be neglected.

The above equations were solved using the finite-element method with the commercial software ABAQUS 6.9-1. The heat transfer model used standard linear three-dimensional wedge-shaped (DC3D6) 6-node brick elements for the sliding plates, hexahedral (DC3D8) 8-node brick elements for the steel band. The stress model used wedge-shaped (C3D6) 6-node linear brick elements for the sliding plates and hexahedral (C3D8R) 8-node linear brick elements for the steel band. This linear thermal and stress problem required about 10 hours to solve on a computer with an 8-core 2.99 GHz Intel Xeon Processor and 16 GB of RAM**.**

HEAT TRANSFER MODEL VALIDATION WITH ANALYTICAL SOLUTION

The model is first validated by solving a simple one-dimensional transient heat transfer problem of conduction through a cylinder, representing preheating of a typical nozzle wall. A schematic of the test problem is shown in Figure 3. Initial, inside, and outside ambient temperatures are all 20 °C; the heat transfer coefficients are 70 W/m^2·K for the inside (combustion gas) and 20 W/m^2·K for the outside (ambient air). The model geometry, properties and constants are given in Figure 3. The exact solution was found using a user friendly spreadsheet-based tool that models heat transfer in submerged entry nozzles during the preheating, cooling down and casting, that was validated previously [6]. The current model simulated a wedge-shaped portion of the nozzle wall with a single layer of 3-D elements with ABAQUS, with all surfaces insulated except for the thin inner and outer boundary surfaces labeled with arrows.

The two solutions match very closely, as shown in Figure 4. The solutions with twenty and forty elements match, thus showing that twenty elements between inside and outside of the nozzle is enough for good spatial resolution. The solutions with time step sizes of every one second and every hundred seconds also match exactly, so that a hundred seconds time step is reasonable. These mesh and time step sizes were used for the sliding gate nozzle model.

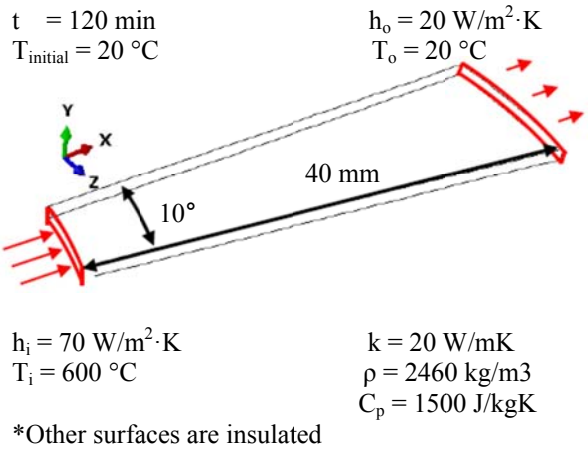

Figure 3. Schematic of boundary condition and properties of test problem

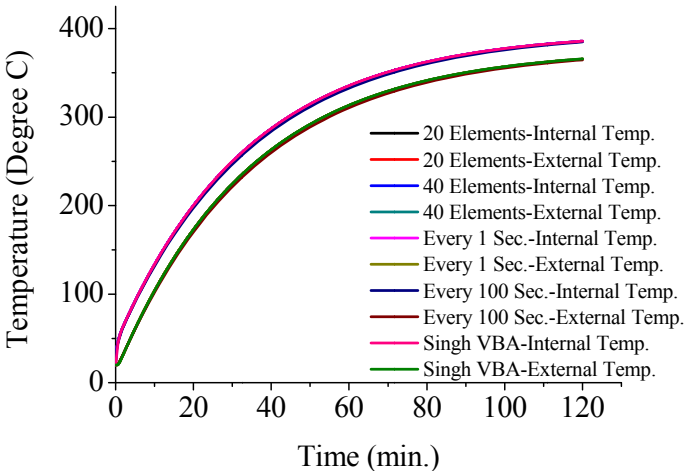

Figure 4. Temperature variation of ABAQUS and S. VBA model

HEAT TRANSFER MODEL VALIDATION WITH EXPERIMENTS

To evaluate the choice of heat transfer boundary conditions, the heat transfer model was next applied to predict transient 3-D heat conduction in a ladle-nozzle plate, and the results were compared with measurements by K. V. Simonov et al. during top teeming of

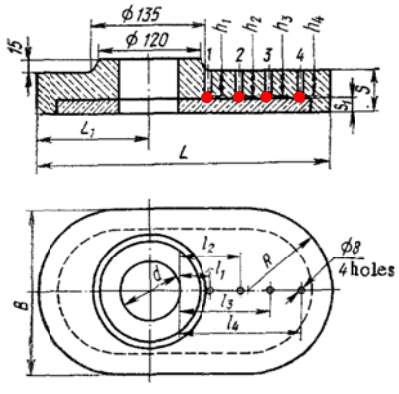

Figure 5. Geometry and thermo-couples location [10]

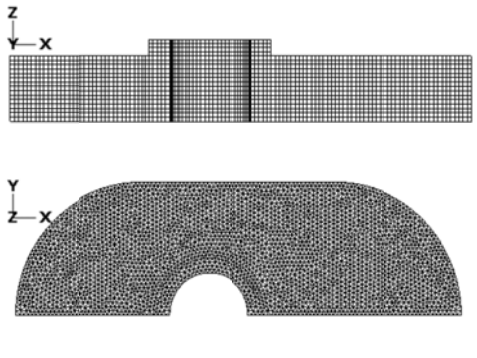

Part	*Element*	
Ladle Plate	(Wedge)	92,378

Figure 6. Finite element mesh and details of ladle plate

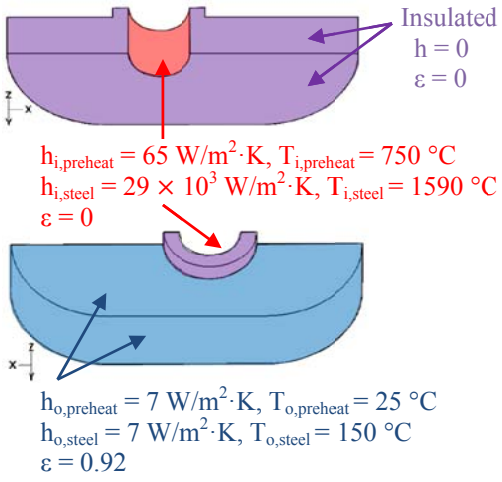

Figure 7. Boundary conditions of ladle plate

molten steel into the mold [10]. Temperatures were measured with four thermocouples installed on the non-working side of the upper plate, and plates were subjected to a preheating thermal treatment at 170 °C.

The geometry and thermocouple locations are shown in Figure 5. Thermocouples are aligned along the plate symmetry plane to measure temperature variation with distance from the inner bore of the plate. A wedge shaped finite element mesh is designed as shown in Figure 6. During the preheating stage, the ladle plate is heated from 25°C with an ambient temperature of 25°C and inside gas temperature of 750 °C, followed by steel casting at 1590 °C, using the same convection coefficients as proposed for the sliding gate nozzle model, and given in Table I. The preheating time was estimated to be 50 minutes, based on when thermocouple number one reached 150°C. Half of the ladle-nozzle plate is simulated, so the symmetry plane is insulated. The contact surfaces between the upper surface of the upper plate and the upper tundish nozzle, the lower surface of the upper plate and the upper surface of the lower plate are also insulated, because it is assumed that the heat exchanged between these surface pairs is negligible (Figure 7). The thermal properties [11] and constants for this ladle plate validation problem are given in Table I.

Table I. Properties[11] and constants for ladle plate model validation problem

Property or Constant	*Value*	
Initial nozzle temp., $T_{initial}$	25	°C
Initial gas temp., $T_{i,preheat}$	750	°C
Internal conv. heat transfer coeff., $h_{i,preheat}$	65.24	W/m^2·K
External ambient temp., $T_{o,preheat}$	25	°C
External conv. heat transfer coeff., $h_{o,preheat}$	7	W/m^2·K
Molten steel temp., $T_{i,steel}$	1590	°C
Internal conv. heat transfer coeff., $h_{i,steel}$	2.87×10^4	W/m^2·K
External ambient temp., $T_{o,steel}$	150	°C
External conv. heat transfer coeff., $h_{o,steel}$	7	W/m^2·K
Density, ρ	3200	kg/m^3
Thermal conductivity, k	8.26	W/m·K
Specific heat, C_p	1004.64	J/kg·°C
Stefan-Boltzmann const., σ	5.37×10^{-8}	W/m^2·K^4
Emissivity[12], ε	0.92	

The upper ladle plate temperature contours predicted by the current ABAQUS model after ninety minutes are shown in Figure 8. Temperature in the plate decreases radially from the plate inner bore to the outside surface with a large, nonlinear temperature gradient due to the large heat capacity of the refractory. Experimental measured and predicted ladle plate temperature histories are compared in Figure 9.

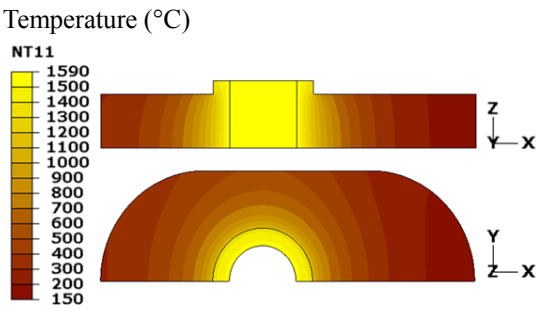

Figure 8. Ladle plate temperature contour, 90 min

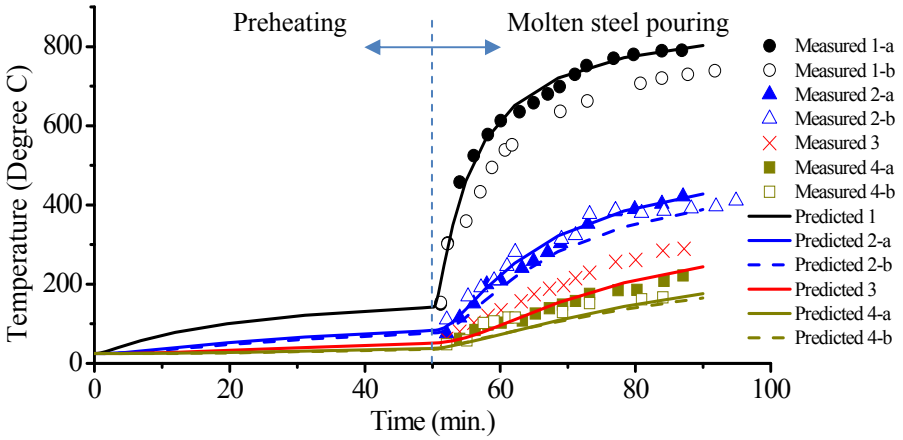

Figure 9. Comparison of measured and predicted temperature in ladle plate

During the forty minutes of casting where thermocouples were recording, the experimental and predicted temperatures in the ladle plate match well with the model simulation, especially near the plate bore. This suggests that assuming an internal gas temperature of 750 °C during preheating is reasonable, in addition to the heat transfer coefficients used for the tundish sliding gate nozzle application.

APPLICATION TO TUNDISH SLIDING GATE NOZZLE PLATES

The half of the symmetrical tundish sliding gate nozzle system assembly simulated in this work is shown in Figure 10. The upper and lower cassette and three sliding-gate plates are all clamped together by four bolts. Each of the plates is surrounded with a steel band and is restrained within the cassette by guide points. The middle plate moves back and forth between such guides which are connected to a hydraulic cylinder to control the molten steel flow. Details of the finite element mesh are shown in Figure 11 and Table II. Three plates and three steel bands are modeled and number of the total elements is 52,871.

Starting initially at ambient temperature, all of the parts are preheated to 750 °C at 100 percent (fully open) for 3.5 hours. Then, the middle plate is moved to zero percent open at 25 mm/sec, taking 5 seconds and held for 12 more minutes while steel fills the tundish.

Then, the middle plate is moved again, increasing the opening to 60 percent, for steady casting. The multiple small movements during the continuous casting process are neglected.

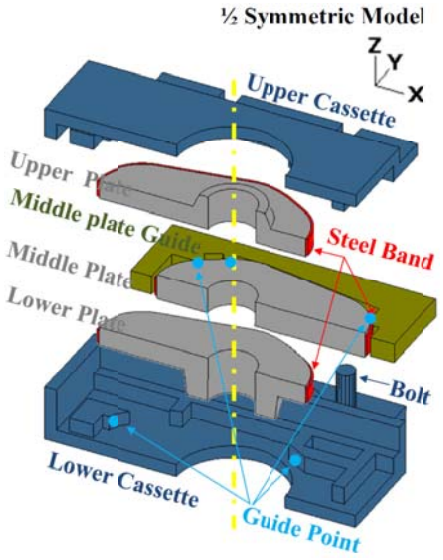

Figure 10. Schematic of tundish sliding gate nozzle assembly

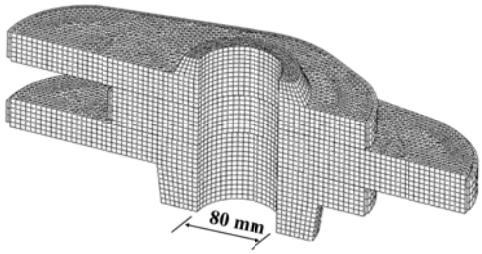

Figure 11. Finite element mesh

Table II. Computational model mesh details

Part	*Elements*	
Upper Plate	(Wedge)	15,133
Middle Plate	(Wedge)	18,008
Lower Plate	(Wedge)	18,782
Upper Band	(Hex.)	512
Middle Band	(Hex.)	512
Lower Band	(Hex.)	384
Total		52,871

After 3.5 hours casting, the opening is moved back to 0 percent. For safety and product quality reasons, the sliding gate nozzle is replaced in the caster every 3.5 hours. The heat transfer model is run for all of these process steps, followed by running the stress model. The properties and constants are shown in Table III.

The boundary conditions of the heat transfer are illustrated in the left side of Figures 12 and 13, for the preheating and continuous casting stages respectively. The boundaries include the inner bore (red regions), outer surfaces (blue regions), and insulated surfaces at the top of the upper plate, bottom of the lower plate and symmetry plane (violet regions). The gap conductance between plates is 0 W/m·K and between each plate and its steel band is 7 W/m·K. For the stress model, illustrated on the right of Figures 12 and 13, the purple regions touch the cassette, upper tundish nozzle (UTN) and submerged entry nozzle (SEN) so the displacement of z-direction is constrained to zero. Grey regions are the contacting guide-points between the cassette and plates, which are constrained in x and y-direction displacement. The side surfaces of the plates (dark blue regions) touch the UTN and SEN, so are constrained in the x and y-directions.

Table III. Properties[11] and constants for sliding gate model

Property or Constant	*Value*	
Initial nozzle temp., $T_{initial}$	25	°C
Initial gas temp., $T_{i,preheat}$	750	°C
Internal conv. heat transfer coeff., $h_{i,preheat}$	65.24	W/m^2·K
External ambient temp., $T_{o,preheat}$	25	°C
External conv. heat transfer coeff., $h_{o,preheat}$	7	W/m^2·K
Molten steel temp., $T_{i,steel}$	1550	°C
Internal conv. heat transfer coeff., $h_{i,steel}$	28719.63	W/m^2·K
External ambient temp., $T_{o,steel}$	150	°C
External conv. heat transfer coeff., $h_{o,steel}$	7	W/m^2·K
Density of refractory, ρ_{ref}	3200	kg/m^3
Thermal conductivity of refractory, k_{ref}	8.26	W/m·K
Specific heat of refractory, $C_{p,ref}$	1004.64	J/kg·°C
Emissivity of refractory[12], ε_{ref}	0.92	
Density of steel, ρ_{steel}	7860	kg/m^3
Thermal conductivity of steel, k_{steel}	48.6	W/m·K
Specific heat of steel, $C_{p,steel}$	418.6	J/kg·°C
Emissivity of steel[12], ε_{steel}	0.75	
Stefan-Boltzmann const., σ	5.37×10^{-8}	W/m^2·K^4

Figure 14 and 15 show contours of temperature and stress during the preheating and continuous casting stages. Temperature in the plates increases sharply from the plate outside surface to the inner bore in the radial direction, especially during the casting stage, when temperature differences between inside and outside are greatest. This generates great thermal expansion near the plate bore, which is constrained by the small amount of expansion in the outside of the plate. This generates compressive hoop stress near the inner bore, which is balanced by simultaneous tension hoop stress towards the outside. At the same time, general expansion of the plate pushes against the guide points, generating radial compression, and extra localized tensile hoop stress.

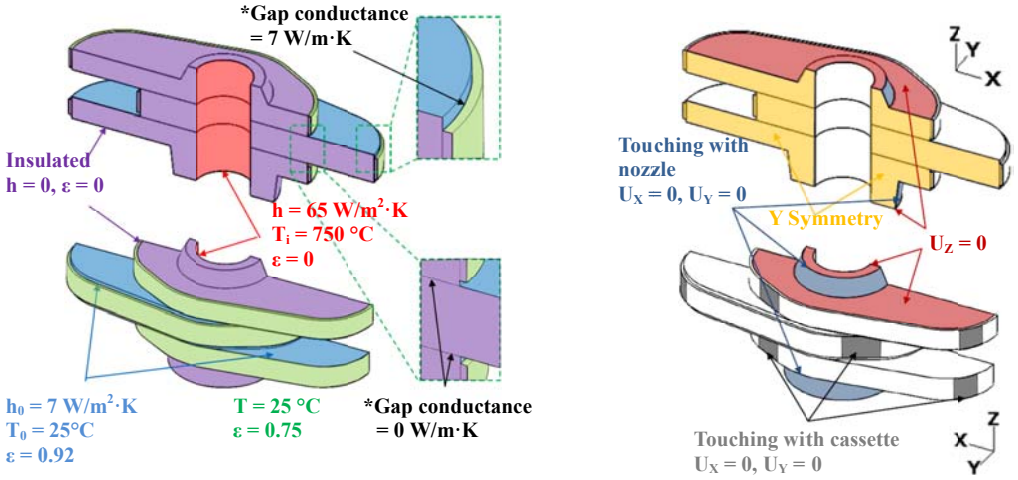

Figure 12. Boundary conditions of heat transfer and stress model in preheating stage

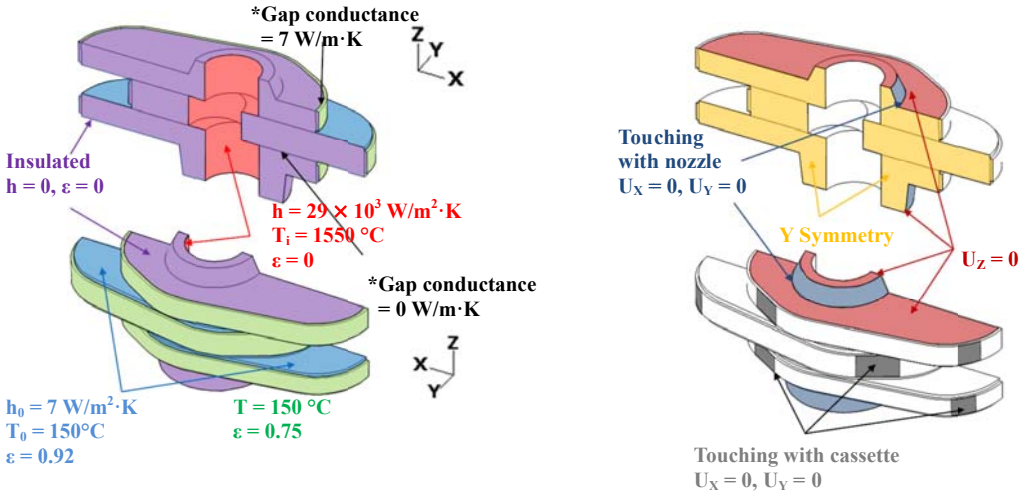

Figure 13. Boundary conditions of heat transfer and stress model in continuous casting stage

The predicted principal stresses are shown in a top-view of the middle plate in Figures 16 and 17, and compared with the location of common through-thickness cracks below. The results suggest two different cracking mechanisms. The excellent agreement between the location of maximum tensile stress on the plate exterior at the location of common observed through-thickness cracks in Figure 16 confirms one mechanism of crack formation. Thermal expansion during heating causes compression near the inner bore, and balancing tension in the exterior of the refractory plate. The maximum principal hoop stress near the thickest part of the plate exceeds the tensile strength of the refractory. The cracks likely formed at these points and propagated inwards, perpendicular to the stress direction, from the outside to the inner bore. Tensile strength of the refractory is not available, owing to its high brittleness. Refractory hand books

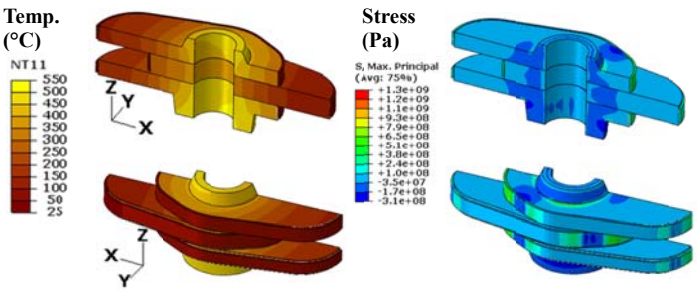

Figure 14. Thermo and mechanical behavior in preheating stage

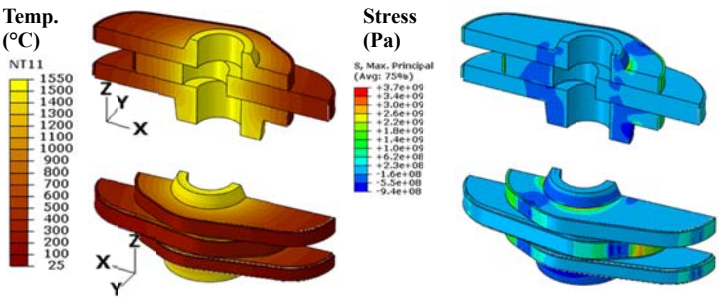

Figure 15. Thermo and mechanical behavior in continuous casting stage

suggest that the tensile strength is about 5 percent of the compressive strength in refractory materials [13]. This stress is exceeded after only 10 minutes of preheating. As time and temperature increase during preheating, the stress gradually increases. Tensile stress during the casting is even higher.

A second common location of through-thickness cracks matches with the location of maximum compressive stress at the refractory surface in Figure 17, where the plate sides contact the cassette guide points. Here, the hoop stress exceeds the compressive strength. This second cracking mechanism depends on the plate shape and cassette guide point location. The time of crack formation is not certain, however. It is possible that this highly-compressed region generated excessive creep in compression, which then generated large tensile stress, and accompanying tensile cracks, during the final cooling-down stage after casting. It is clear that guide-point geometry design and clamp forces must be optimized to lower this compressive stress to prevent this mechanism of plate cracking.

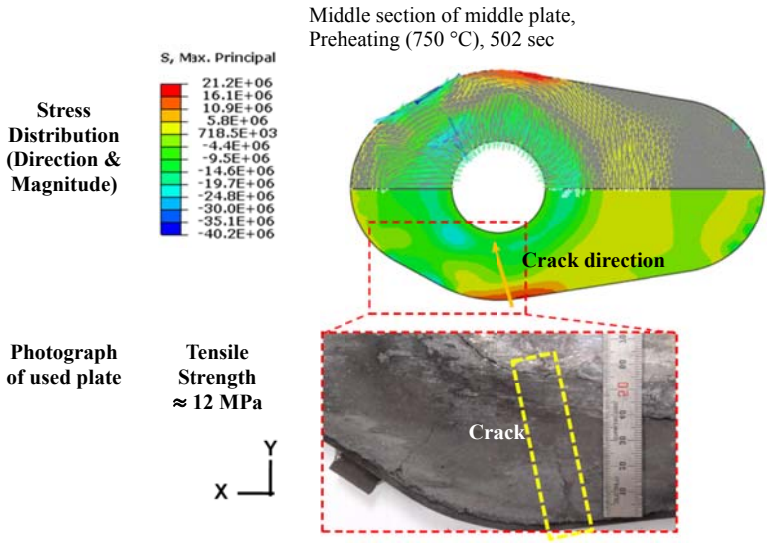

Figure 16. Common through-thickness crack formation mechanism of tensile stress

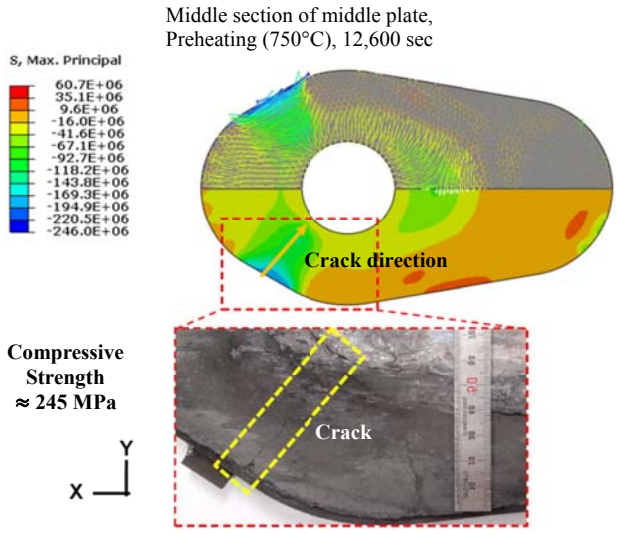

Figure 17. Common through-thickness crack formation mechanism of compressive stress

CONCLUSIONS

This paper investigates the thermal and mechanical behavior of tundish sliding gate nozzle plates during preheating and continuous casting, using a three-dimensional finite-element model. The internal gas temperature and heat transfer coefficients are calculated using previous models and theory. The heat-transfer model and its boundary conditions are validated with an analytical test problem, and with previous experimental temperature measurements of a ladle-nozzle plate. The tundish sliding gate nozzle model predicts that during the preheating stage, the tensile and compressive stresses exceed both the refractory tensile and compressive strengths. The model predictions of the maximum stress locations and orientation match well with the crack locations observed in used plates. This suggests two different cracking mechanisms which are both observed in practice. Thermal expansion due to the temperature variations are the first important mechanism causing cracks to form in the plate due to tensile stress during heating stages. Secondly, geometrical design of the cassette appears to constrain the plates to apply excessive pressure at the cassette guide points during operation. The cassette is an important part of the model prediction of crack formation, and the geometry of its guide points should be optimized to prevent cracks due to excessive compression. Further work is needed to incorporate the effects of creep and residual stress, to better investigate crack formation.

ACKNOWLEDGEMENTS

The authors wish to thank the Continuous Casting Consortium at the University of Illinois at Urbana-Champaign as well as colleagues in the Clean Steel and Non-ferrous Metals Processing Laboratory, POSTECH. Thanks are also given to Sung-Kwang Kim – POSCO Kwangyang works and Kwon-Myung Lee – POSCO Pohang works. Financial support from POSCO (Grant No. 4.0007764.01) is gratefully acknowledged.

REFERENCES

1. Munteanu, V., *Steel and Refractory Chemical Interactions and Mechanical Behavior of Plates for Sliding Gate during Steel Continuous Casting.* The Annals of "Dunarea de Jos" University of Galati. Fascicle IX. Metallurgy and Materials Science, 2008. **No.2-2008**: p. 32-36.
2. Jayanta Chaudhuri, G.C., Satyendra Kumar, Visvanathan V. Rajgopalan, *New Generation Ladle Slide Gate System for Performance Improvement.* MPT International, 2007. **30**(No. 6): p. 38-42.
3. Zhi-He Jin, Y.-W.M., *Effects of Damage on Thermal Shock Strenth Behavior of Ceramics.* Journal of American Ceramic Society, 1995. **78**(7): p. 1873-1881.
4. Lance C. Hibbeler, B.G.T. *Thermal Distortion of Funnel Molds*. in *AISTech*. 2011. Indianapolis, Ind., USA.
5. *Korea Gas Safety Corporation*.
6. Varun Kumar Singh, B.G.T., *User Friendly Model of Heat Transfer in Submerged Entry Nozzles during Preheating, Cool Down and Casting*, in *Continuous Casting Consortium*2010: University of Illinois at Urbana-Champaign.
7. Stuart W. Churchill, H.H.S.C., *Correlating Equations for Laminar and Turbulent Free Convection from a Vertical Plate.* International Journal of Heat and Mass Transfer, 1975. **18**(9): p. 1323-1329.
8. Incropera, F.P., and Dewitte, P. D., *Fundamentals of Heat and Mass Transfer*2002, New York: John Wiley and Sons.
9. C. A. Sleicher, M.W.R., *A convenient correlation for heat transfer to constant and variable property fluids in turbulent pipe flow.* International Journal of Heat and Mass Transfer, 1975. **18**(5): p. 677-683.
10. K. V. Simonov, S.I.R., A. A. Kortel', L. A. Reinov, *Thermal Loading of Periclase Plates in Sliding Gates of Steel-teeming Ladles.* Refractories and Industrial Ceramics, 1979. **20**: p. 742-746.
11. *Chosun Refractories Co. Ltd. Research Center*.
12. *Monarch Instrument "Table of Emissivity"*.
13. Schacht, C.A., *Refractories Handbook*2004, Cimarron Rd., Monticello, NY 12701, USA 800-228-1160: Marcel Dekker, Inc